Pulsed upconversion imaging of mid-infrared supercontinuum light using an electronically synchronized pump laser

Huot, Laurent; Moselund, Peter Morten; Tidemand-Lichtenberg, Peter; Pedersen, Christian

Published in:
Applied Optics

Link to article, DOI:
10.1364/AO.58.000244

Publication date:
2019

Document Version
Peer reviewed version

Pulsed upconversion imaging of mid-infrared supercontinuum light using an electronically synchronized pump laser

LAURENT HUOT[1,2,*], PETER MORTEN MOSELUND[1], PETER TIDEMAND-LICHTENBERG[2], AND CHRISTIAN PEDERSEN[2]

[1] NKT Photonics A/S, Blokken 84, 3460 Birkerød, Denmark
[2] DTU Fotonik, Frederiksborgvej 399, 4000 Roskilde, Denmark
[*] Corresponding author: lhu@nktphotonics.com

In this paper, a versatile method for synchronized imaging upconversion in the mid-IR wavelength range is presented. A 1064 nm MOPA source pump laser is electronically adjusted in pulse duration and repetition rate to match the output from a 40 kHz, 1.6 ns pulses mid-IR supercontinuum light source followed by upconversion to the near-infrared captured by a sensitive CCD camera. The systems noise is characterized and we present a simple algorithm for correcting for the image distortion caused by the use of off-axis parabolic mirrors.

1. INTRODUCTION

In recent years, mid-infrared (mid-IR) sources like broadband supercontinuum sources and tunable quantum cascade lasers have received a lot of interest for their strong potential for novel spectroscopy and imaging applications [1–3]. However, developing fast, low-noise detectors in this wavelength range remains a major challenge. Usually, mid-IR detectors are based on low bandgap semiconductor materials like indium antimonide (InSb) or mercury cadmium telluride (HgCdTe). Alternatively, microbolometer arrays and thermopiles are used. All these detectors suffer from inherent dark noise and require cooling to perform optimally [4]. These detection systems are usually expensive or have slow response times that make them unsuitable for many applications. Upconversion detection circumvents these complications by converting the mid-IR signal to the visible or near-infrared range. This is achieved through nonlinear parametric sum-frequency mixing in a $\chi^{(2)}$ medium. The upconverted signal can then be acquired on a standard silicon-based detector which are known to work with much lower noise and faster temporal performance than their mid-IR counterparts and cost significantly less.

The upconversion process, being a nonlinear parametric process, greatly benefits from being implemented in a pulsed setup. The high peak power of the conversion pump pulses ensures efficient upconversion of the mid-IR signal pulses and eliminates the need for an intracavity system [5]. A single-pass setup with synchronous pumping [6] relaxes the demanding constraints for the nonlinear material to have high nonlinearity and low transmission losses. This allows the use of bulk crystals which can easily be manufactured in sizes of the order of several mm. Their larger aperture permits the use of a large beam diameter in the nonlinear crystal which increases spatial resolution [7]. Moreover, supercontinuum sources further in the mid-IR spectrum may be upconverted using a similar method exploiting crystals like $AgGaS_2$ or $AgGaSe_2$. Additionally, thermal noise being proportional to the average pump power, pulsed upconversion systems are far less sensitive to thermal noise than continuous wave upconversion setups since they generally operate at much lower average pump powers [8].

An imaging system based on this principle was previously demonstrated in [6] and relied on a single 1550 nm laser source to pump both the supercontinuum extending up to 4.5 µm and the upconversion process. Unfortunately, with these wavelengths the sum-frequency signal ranged from 1030 nm to 1155 nm and required the use of an InGaAs based detector to acquire the upconverted signal. Since, active electronic delay tuning has been shown to be a simple and effective method for synchronizing optical pulses for upconversion [9]. The temporal stability of the system was a mere 48 ps (jitter) and with low drift over time, thus no active locking mechanism was needed when operated in the ns regime. Besides facilitating time resolved measurements, this method gives the operator the freedom to independently choose the wavelengths of the pump and infrared signal wavelengths to best suit the application.

In this paper, we exploit this feature by synchronizing a 1064 nm MOPA with electronically adjustable pulse duration and rep-

etition rate to match a 40 kHz supercontinuum laser with 1.6 ns pulse duration. As a consequence the upconverted wavelengths end up in the attractive 650 nm to 850 nm wavelength range where standard silicon CCD cameras can be used. The proposed architecture is general in nature and can be implemented with different illumination sources. We employ in this paper a simple achromatic upconversion imaging setup using off-axis parabolic mirrors. The performance of the system is characterized in terms of imaging quality and noise.

2. EXPERIMENT

The experiment is based on the setup from [9] and is represented in Fig. 1. The externally triggered supercontinuum emits 1.6 ns pulses at 40 kHz repetition rate and its spectrum ranges from 1.8 µm to 4.2 µm [10]. For the measurement integration times used throughout this study, the polarization noise of the source can be neglected due to averaging over multiple pulses [11]. Thus, the supercontinuum light can be considered randomly polarized throughout its spectrum. The spectrum of the supercontinuum is shown in Fig. 2. The supercontinuum light is filtered through a 2 µm long pass filter (LPF1). The average power of the full supercontinuum between 2 µm and 4.2 µm is 24 mW and its spectrum can be considered spatially uniform. The light is then collimated to a 15 mm diameter beam using a 50.8 mm parent focal length gold coated 30° off-axis parabolic mirror (OAPM 1). It is then tightly focused inside a bulk lithium niobate ($LiNbO_3$) crystal using a 25.4 mm parent focal length 30° OAPM (OAPM 2). These mirrors have a uniform high reflectance in the mid-IR and eliminate chromatic aberration. They however introduce different types of aberration and in particular a keystone distortion that will be addressed subsequently in this paper [12]. The crystal is undoped and of congruent composition. It is 10 mm long, has a 5 mm x 5 mm cross section and is cut for $\theta = 48°$ and $\phi = -90°$. The crystal is used at room temperature, and no temperature stabilization was implemented. It is set at an incidence angle of approximately 0.2° relative to the direction of the pump beam. This angle is kept constant throughout the experiment.

The sum frequency generation is performed according to type I phase matching. The supercontinuum is focused down in the nonlinear crystal and overlapped spatially and temporally with linearly polarized 1064 nm MOPA pulses that serve as the pump for the upconversion process. Both the pump source and the supercontinuum source have a single-mode fiber output and thus the emitted beams can be considered to be Gaussian. Both sources are spatially coherent and thus coherent image upconversion is performed [7]. The direction of the pump laser polarization is adjusted using a half-wave plate to match the ordinary axis of the $LiNbO_3$ crystal. In this configuration, the effective nonlinear coefficient is approximately $d_{eff} = 4.3$ pm/V. The pump laser produces 1 W of average power and is based on a MOPA architecture seeded by a gain switched DFB diode [13]. The duration of the MOPA pulses is set to 1.6 ns FWHM to match the duration of the supercontinuum pulses. The pump light is first collimated with a 7.5 mm focal length aspheric lens (L1) and spatially overlapped with the supercontinuum focus inside the nonlinear crystal. By placing a camera at the crystal position, the pump beam profile was measured to be that of a 1.6 mm $1/e^2$ diameter Gaussian beam. With these parameters, the maximum quantum efficiency, found for narrowband illumination satisfying the phase matching condition, is estimated to be of the order of 1%. It is of interest to note that the quantum

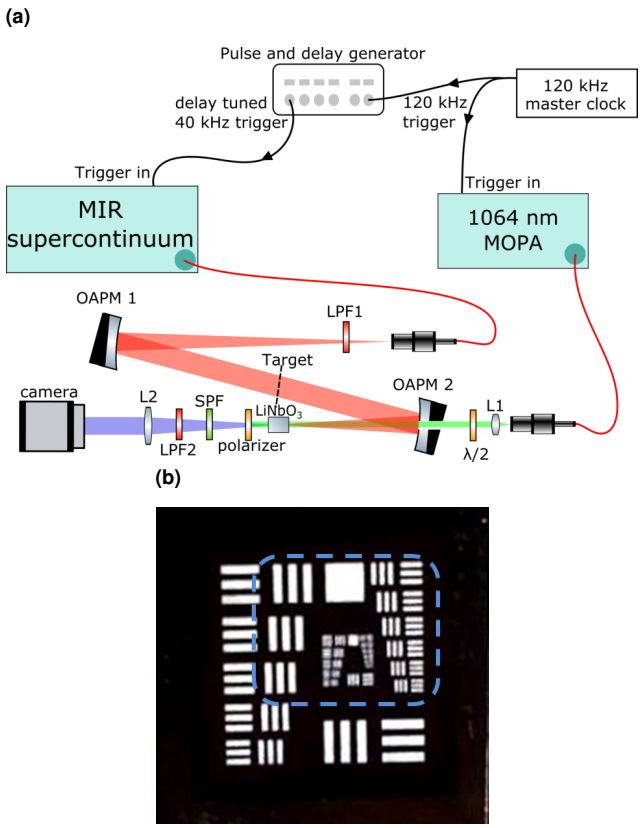

Fig. 1. (a) Schematic representation of the experimental setup. L1 : 7.5 mm aspheric lens, L2 : 50 mm plano-convex lens, OAPM 1 : 50.8 mm parent focal length 30° gold coated OAPM, OAPM 2 : 25.4 mm parent focal length 30° gold coated OAPM, LPF1 : 2 µm long-pass filter, LPF2 : 650 nm long-pass filter SPF : 850 nm short-pass filter. (b) Clear optical path USAF 1951 resolution test target.

efficiency of the upconversion scales linearly with the pump peak power, and that the pump peak power of could in theory be scaled to increase the quantum efficiency. Note that a 3 mm diameter hole was drilled in OAPM2 along the axis of the mid-IR focused beam. The pump beam is passed through it and aligned to be coaxial to the mid-IR beam. This is a simple and inexpensive method of combining the broadband mid-IR signal with the pump beam. The presence of the hole causes a part of the image to be obscured as can be seen in Fig. 3(a). The broad field of view of the system is achieved using non-collinear phase matching [14, 15]. The delay between the mid-IR pulses and pump pulses was scanned using the Highland technologies T560 digital delay and pulse generator [9]. The conversion is maximized through the temporal overlap.

After the crystal, the light is filtered through a polarizer transmitting the upconverted signal while blocking the pump laser, a 850 nm short-pass filter (SPF) and a 650 nm long pass filter (LPF2) and the upconverted light is collected with a 50 mm focal length plano convex lens (L2) and acquired on an Andor Technologies $Luca^{EM}$ S 658M camera with a silicon-based CCD sensor. The target, OAPM2, collection lens L2 and camera sensor are placed so as to form a 4f setup [7]. It is important to note that the focal length of OAPM2 is not constant across its surface, and thus the target has to be tilted a couple of degrees with respect to the collimated supercontinuum beam. The angular position

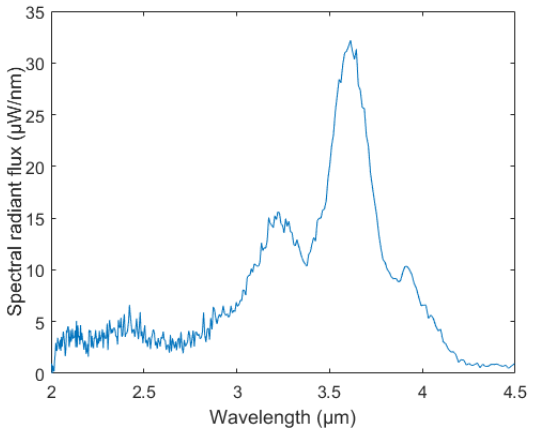

Fig. 2. Spectral radiant flux of the supercontinuum source

of the target was optimized to achieve the sharpest possible image across the entire field of view. The angle being shallow and the target being thin, this tilting of the object plane does not cause any shadowing effects in the object. Figure 1(b) shows the clear optical path USAF 1951 resolution test target used to assess the imaging quality. The supercontinuum light illuminates the target with a 15 mm diameter gaussian intensity profile.

3. RESULTS

Figure 3(a) is a raw camera image obtained when no target is inserted. The dark circle is due the the hole in OAPM2. The distribution of wavelengths in the upconverted image is dictated by non-collinear phase matching [14]. The theoretical distribution of wavelengths can be seen in Fig. 3(b), 3(c). The shortest wavelengths are in the center of the image while the longer wavelengths appear as rings of varying radius. It is important to note that the wavelength range used in this experiment spans beyond the inflexion point in the phase matching condition, which causes multiple wavelengths to be upconverted in the same position in the image plane [16]. This causes blurring in the imaging along the outer most rings as the magnification of the system varies with wavelength. As mentioned subsequently, this ambiguity of the wavelengths in outer part of the image also prevents proper operation of our rescaling algorithm. If necessary, this ambiguity can be solved by placing a short-pass filter at the inflexion wavelength. Additionally, the very bright ring on the outer edge of the image is due to the peak around 3.6 μm in the spectrum of the supercontinuum that can be seen in Fig. 2 combined with an increased spectral acceptance bandwidth close to the inflexion point. Finally, close to the outher edge of the image, a dark ring is present. This could be due to an absorption feature in the setup. Unfortunately, due to the uncertainty on the corresponding wavelength due to the ambiguity of the wavelengths caused by the inflexion point the cause of the feature could not be identified.

Figure 4(a) shows the raw upconverted image that the system can generate. The images hold barrel distortion due to the wavelength dependent angular magnification in non-collinear phase matching [7, 14]. Additionally, the figures also bear horizontal keystone distortion (features on the right of the image appear more magnified than features on the left) due to the use of the second off-axis parabolic mirror. It can be shown that the upconverted image is a replica of the original image scaled with

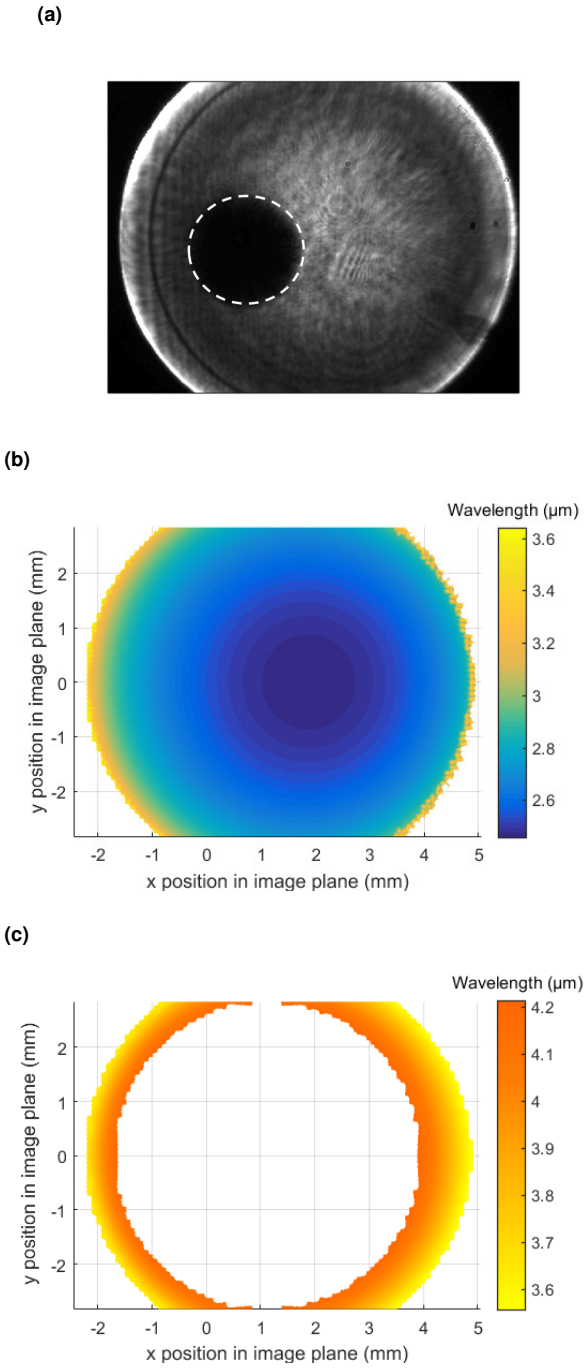

Fig. 3. (a) Raw camera image when the resolution target is removed from the object plane. The white dashed circle delimits the area obscured due to the hole in OAPM2. (b) Distribution of wavelengths below the phase matching inflexion point. (c) Distribution of wavelengths above the phase matching inflexion point.

a factor M expressed in eq. (1)

$$M = -\frac{\lambda_3 f_2}{\lambda_1 f_1} \tag{1}$$

λ_3 and λ_1 are the wavelengths of the upconverted and input beams respectively, f_1 is the focal length of OAPM2 and f_2 is

the focal length of lens L2 [17]. The scaled image is further convolved with the point spread function defined by the beam size of the pump laser. However, the focal length f_1 of the OAPM varies across the surface of the mirror according to the equation of a paraboloid. Thus, for every beam section reflected by the mirror with an angle θ with respect to the axis of symmetry of the paraboloid, the focal length f_1 can be expressed simply as in eq. (2), where f_{parent} is the parent focal length of OAPM2 [12].

$$f_1(\theta) = -\frac{2f_{parent}}{1 + cos(\theta)} \quad \textbf{(2)}$$

The spatial distribution of wavelengths in both the input infrared signal and the upconverted image is calculated according to non-collinear phase matching and thus all the parameters of the scaling factor M are known. A rescaling algorithm was devised and implemented as a Matlab script. For each pixel coordinate of the distorted input image, the scaling factor M is calculated. By applying the factor 1/M to each pixel coordinate, a new set of pixel coordinates describing the position of said pixels in the object plane is generated. This set of scattered pixel coordinates is then resampled to a standard two-dimensional image matrix by using Matlab's built in "griddata" interpolation function. Figure 4(b) shows the image after it has been rescaled by the scaling factor 1/M. The dashed line marks the limit within which the image correction algorithm is applicable, and thus our effective field of view. For the parameters given in this experiment, the field of view is a circular disc 13 mm in diameter, with a 3 mm diameter obscured section caused by the hole in OAPM1. Within this boundary the resized image is in good overall agreement with the target and any discrepancies can be attributed to misalignments. Outside of the dashed boundary we notice deformations of the image due to multiple wavelengths above and below the inflexion point of the crystal being upconverted at the same phase match angles. It is important to note, that rotating the nonlinear crystal will change the spatial distribution of phase matched wavelengths and thus the field of view. Here the angle was adjusted in order to match the field of view to our camera sensor size.

We also measured the resolution limit close to the center of the rescaled image. Figure 5 shows a pixel-value cross-section of the image along the features of group 3 of the resolution target. The location of these features is indicated in 4(b) by a vertical dotted arrow. Element 5 is resolved while element 6 is not according to the Rayleigh criterion. Thus the resolution limit is between 78.8 µm and 70.2 µm. In order to calculate the theoretical resolution limit, we first calculated the resolution limit imposed by the finite size of the pump beam in the case of incoherent mid-IR illumination. Assuming that the phase of the light at the object plane is constant, the resolution for coherent mid-IR illumination is worse than the incoherent case by a factor $\sqrt{2}$ [17]. The theoretical resolution limit was calculated to be 56 μm according to the size of the pump beam [17]. The difference between the theoretical and experimental value can be largely attributed to aberration introduced by the use of OAPMs and uncertainty of the pump beam size.

It has been shown that upconversion imaging and spectroscopy can be prone to thermal noise [8]. We investigated the variation of the intensity noise in each pixel as a function of integration time. For a given integration time, 100 camera frames are acquired first when both the supercontinuum and pump beams are blocked, then when only the blocking the supercontinuum, and finally when both beams are active. The

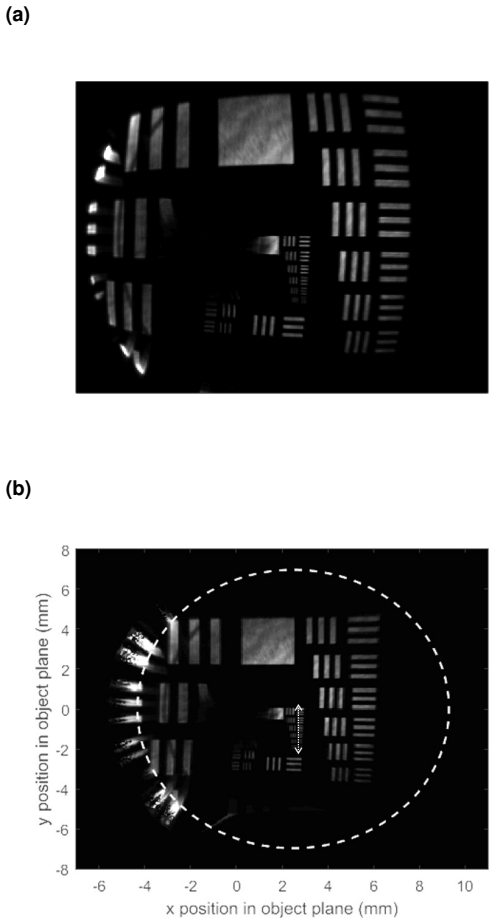

Fig. 4. (a) Raw camera image of the resolution target. (b) Distortion corrected and scaled image of the resolution target. A white dotted arrow marks the location of the image cross-section showed in Fig. 5

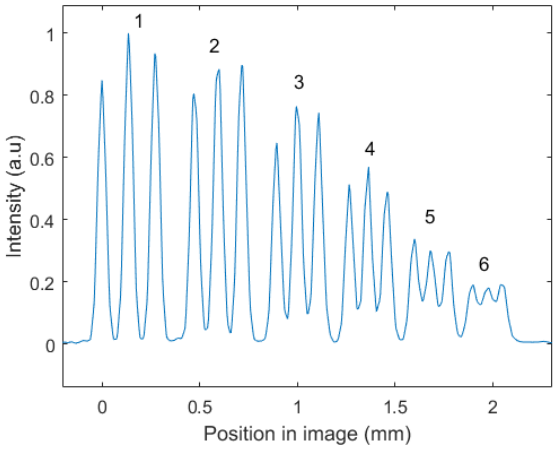

Fig. 5. Pixel-value cross-section along a a vertical line across group 3 in the corrected image. The numbers above the features denote the corresponding number of the elements within the group. The horizontal axis refers to dimensions of the rescaled image in the object plane.

variation of count rates per pixel was calculated. These measurements were performed for integration times ranging from 0.5 ms to 150 ms. The noise introduced by the camera is constant throughout the image and does not vary with integration time as it is dominated by the sensor readout noise. When only the pump laser is switched on, a small portion of the 1064 nm light leaks through the filters and gets detected by the camera as a small bright spot in the center of the obscured part of the image. No additional noise is introduced in the image and, even at the longest integration times, no thermal noise is observed. This is due to the low average power of the pump system compared to continuous-wave pumped intra-cavity upconversion systems which typically operate at much higher average power [8]. Finally, when the sources are switched on, the noise contribution of the upconverted light is simply added to the camera readout noise as both noise sources are independent.

Figure 6 shows the variance of the pixel counts as a function of integration time for 5 different wavelengths in the upconverted image. For all wavelengths, the variance increases linearly with time which indicates that the noise is limited by shot noise from the signal. The slope of the plots is proportional to the brightness of the upconverted signal at the corresponding wavelengths which is a product of of the spectral brightness of the supercontinuum source combined with the angular dependent efficiency of the upconversion process. Note that the variance evolves linearly even at the shortest integration times and that the pulse to pulse noise of the supercontinuum source does not appear to have any influence at the integration times. Indeed, with a repetition rate of 40 kHz, even at the shortest integration time of 0.5 ms, the images are averaged over 20 supercontinuum pulses which is enough to make the influence of pulse to pulse fluctuations negligible compared to shot noise from the signal. Last but not least, for an integration time of 0.5 ms, the noise variance of the upconverted signal is approximately equal to the camera readout noise variance and thus at this integration time the signal to noise ratio is close to 1.

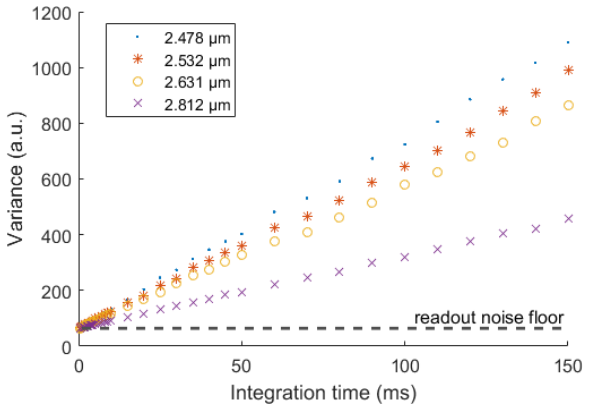

Fig. 6. Evolution of the total intensity variance at given wavelengths as a function of camera integration time.

4. CONCLUSION

In this paper, a pulsed upconversion imaging system relying on active electronic synchronization was presented. Mid-IR pulses from a supercontinuum source were electronically synchronized with pulses from 1064 nm MOPA pump source and upconverted in bulk lithium niobate in a single-pass imaging setup. This detection scheme was shown to be shot noise limited mainly due to the pulsed nature of the pump, minimizing the thermal noise while conserving high quantum efficiency. A simple rescaling algorithm correcting for distortion induced by the use of OAPMs was demonstrated and the spatial resolution of the system was measured to be better than 78.8 µm at a wavelength of 2.5 μm. This method could be adapted for use with different mid-IR light sources like quantum cascade lasers and the versatility of the electronic synchronization could prove to be an invaluable tool for frequency conversion applications across the mid-IR. Additionally, this system can be modified similarly to the experiment presented in [18] in order to perform measurements in diffuse reflection rather than in transmission.

FUNDING INFORMATION

The Mid-TECH project has received funding from the European Union's Horizon 2020 research and innovation programme under Grant Agreement No. 642661.

REFERENCES

1. R. F. Curl, F. Capasso, C. Gmachl, A. A. Kosterev, B. McManus, R. Lewicki, M. Pusharsky, G. Wysocki, and F. K. Tittel, "Quantum cascade lasers in chemical physics," Chem. Phys. Lett. **487**, 1 – 18 (2010).
2. A. B. Seddon, T. M. Benson, S. Sujecki, N. Abdel-Moneim, Z. Tang, D. Furniss, L. Sojka, N. S. ad Nallala Jayakrupakar, G. R. Lloyd, I. Lindsay, J. Ward, M. Farries, P. M. Moselund, B. Napier, S. Lamrini, U. Møller, I. Kubat, C. R. Petersen, and O. Bang, "Towards the mid-infrared optical biopsy," ProcSPIE **9703**, 970302 (2016).
3. J. Kilgus, K. Duswald, G. Langer, and M. Brandstetter, "Mid-infrared standoff spectroscopy using a supercontinuum laser with compact fabry–pérot filter spectrometers," Appl. Spectrosc. **72**, 634–642 (2018). PMID: 29164925.
4. A. Rogalski, *Infrared Detectors* (CRC Press, 2011).
5. S. Dupont, P. M. Moselund, L. Leick, J. Ramsay, and S. R. Keiding, "Up-conversion of a megahertz mid-ir supercontinuum," J. Opt. Soc. Am. B **30**, 2570–2575 (2013).
6. L. Huot, P. M. Moselund, L. Leick, P. Tidemand-Lichtenberg, and C. Pedersen, "Broadband upconversion imaging around 4 μm using an all-fiber supercontinuum source," ProcSPIE **10088**, 100880J (2017).
7. C. Pedersen, E. Karamehmedović, J. S. Dam, and P. Tidemand-Lichtenberg, "Enhanced 2d-image upconversion using solid-state lasers," Opt. Express **17**, 20885–20890 (2009).
8. A. Barh, P. Tidemand-Lichtenberg, and C. Pedersen, "Thermal noise in mid-infrared broadband upconversion detectors," Opt. Express **26**, 3249–3259 (2018).
9. L. Huot, P. M. Moselund, P. Tidemand-Lichtenberg, and C. Pedersen, "Electronically delay-tuned upconversion cross-correlator for characterization of mid-infrared pulses," Opt. Lett. **43**, 2881–2884 (2018).
10. V. V. Alexander, O. P. Kulkarni, M. Kumar, C. Xia, M. N. Islam, F. L. Terry, M. J. Welsh, K. Ke, M. J. Freeman, M. Neelakandan, and A. Chan, "Modulation instability initiated high power all-fiber supercontinuum lasers and their applications," Opt. Fiber Technol. **18**, 349 – 374 (2012).
11. J. Ramsay, S. Dupont, and S. Keiding, "Pulse-to-pulse noise reduction in infrared supercontinuum spectroscopy: polarization and amplitude fluctuations," Laser Phys. Lett. **11**, 095702 (2014).
12. J. E. Howard, "Imaging properties of off-axis parabolic mirrors," Appl. Opt. **18**, 2714–2722 (1979).
13. S. Kanzelmeyer, H. Sayinc, T. Theeg, M. Frede, J. Neumann, and D. Kracht, "All-fiber based amplification of 40 ps pulses from a gain-switched laser diode," Opt. Express **19**, 1854–1859 (2011).
14. P. Tidemand-Lichtenberg, J. S. Dam, H. V. Andersen, L. Høgstedt, and C. Pedersen, "Mid-infrared upconversion spectroscopy," J. Opt. Soc. Am. B **33**, D28–D35 (2016).

15. A. J. Torregrosa, H. Maestre, and J. Capmany, “Intra-cavity upconversion to 631 nm of images illuminated by an eye-safe ase source at 1550 nm,” Opt. Lett. **40**, 5315–5318 (2015).
16. A. Barh, C. Pedersen, and P. Tidemand-Lichtenberg, “Ultra-broadband mid-wave-ir upconversion detection,” Opt. Lett. **42**, 1504–1507 (2017).
17. J. S. Dam, C. Pedersen, and P. Tidemand-Lichtenberg, “Theory for upconversion of incoherent images,” Opt. Express **20**, 1475–1482 (2012).
18. N. Sanders, L. Kehlet, J. S. Dam, P. Tidemand-Lichtenberg, P. Beato, and C. Pedersen, “Mid infrared upconversion spectroscopy using diffuse reflectance,” ProcSPIE **8964**, 8964 – 8964 – 7 (2014).